Evaluation by nanoindentation of the influence of heat treatments and the consequent induced microstructure on the mechanical response of the heat-treated L-PBF AlSi10Mg alloy

G. Di Egidio

The hierarchical microstructure of the AlSi10Mg alloy produced by the Laser-based Powder Bed Fusion (L-PBF) determines peculiar microstructural and mechanical characteristics. The scientific literature reports generic correlations between the main microstructural features and the mechanical behavior of the alloy, bypassing however the analysis of the effects of the sub-structure on the local mechanical behavior. The present study, therefore, used the nanoindentation technique to determine the influence of different heat treatment conditions on the sub-structure and local mechanical properties of the L-PBF AlSi10Mg alloy. In particular, the following heat treatments were considered: T5 (160 °C for 4 h), T6B (540 °C for 1 h + 160 °C for 4 h), and T6R (510 °C for 10 min + 160 °C for 6 h). The study highlighted how small variations in the morphology or size of the main microstructural characteristics affect the local mechanical behavior, consequently reflecting on the overall mechanical behavior of the material.

KEYWORDS: LASER-BASED POWDER BED FUSION (L-PBF), SELECTIVE LASER MELTING (SLM), AL ALLOY, ALSI10MG, HEAT TREATMENT, NANO-INDENTATION, MICROSTRUCTURE, MECHANICAL PROPERTIES;

INTRODUCTION

The Laser-based Powder Bed Fusion (L-PBF) process plays a leading role in an increasingly flexible and sustainable industrial sector, thanks to greater efficiency in the production of high-value-added components compared to conventional production processes [1-3]. Among the different Al alloys that can be used in the L-PBF applications, the AlSi10Mg alloy is preferred given its good processability, which is due to the almost eutectic chemical composition, the low susceptibility to hot cracking, and the limited solidification range ($\Delta T \approx 50$ °C). Furthermore, the high Mg content allows an increase in its mechanical properties by precipitation of the strengthening phases (Mg_2Si) both in the processing and during the heat treatments [2,4].

The specific process conditions of the L-PBF technology and the chemical-physical properties of the AlSi10Mg alloy determine the formation of a peculiar hierarchical microstructure. They lead to the formation of a Melt Pool (MP) structure within which the growth of epitaxial grains is

Gianluca Di Egidio
Department of Industrial Engineering (DIN), Alma Mater Studiorum, University of Bologna, Viale Risorgimento 4, 40136 Bologna, Italy

promoted by the similarity in crystal structure and chemical composition between the solid substrate and the liquid metal. At the same time, the non-equilibrium solidification conditions, due to the high cooling rate, lead to the formation of an extremely fine subcellular structure consisting of submicrometric cells of supersaturated α-Al matrix surrounded by a eutectic-Si network [3]. The microstructure in the as-built (AB) condition is therefore characterized by different strengthening mechanisms, which induce higher static strength properties (yield strength (YS) and ultimate tensile strength (UTS)) than conventional Al-Si-Mg casting alloys, even if lower elongation to failure (ef) and impact toughness. Therefore, several heat treatments generally used on Al casting alloys have been applied to the L-PBF AlSi10Mg alloy to improve the mechanical properties balance [4].

The T5 heat treatment promotes the precipitation hardening by nanometric Si precipitates and precursors of the equilibrium phase Mg_2Si, also preserving the main strengthening mechanisms of the AB condition (microstructural refinement, solid solution, aggregated second phase). At the same time, it reduces the dislocation density and consequently, the residual stresses in the L-PBF-produced part, thus slightly improving the ef value while maintaining or even increasing the strength properties of the alloy [5]. Conversely, the T6 heat treatment eliminates the MP structure and modifies the substructure which is characterized by a homogeneous distribution of Si particles embedded in an α-Al phase matrix. In this case, the microstructural evolution determines a better balance between the mechanical properties given by an increase in ductility and toughness, and a limited or no decrease in the YS value due to the precipitation hardening that occurs in artificial aging [6].

In the literature [4,7], the role of the arrangement and morphology of the Melt Pool Boundaries (MPB) and the cellular structure size on the ductility and the strength properties of the AB and T5 conditions is widely known. At the same time, in previous work [6] the author showed the effects of the second dispersed phase on the mechanical behavior of the T6 heat-treated AlSi10Mg alloy. In particular, the influence of the shape, morphology, and distribution of the Si particles in the Al matrix on both the strength properties and the ductility of the T6 alloy was highlighted.

However, to the best of the author's knowledge, a detailed analysis of the effects of the substructure on local mechanical behavior is lacking in the literature. For example, Moses et al. [7] and Zhuo et al. [8] performed nanoindentation tests on AB and heat-treated samples, however, without reporting neither a precise mapping of the influence of the different phases and features that characterize the microstructure of the L-PBF AlSi10Mg alloy, nor a direct correlation between local and macroscopic mechanical properties.

This lack of knowledge led to the investigation, by nanoindentation tests, of the correlations between local mechanical behavior and microstructural features of the heat-treated L-PBF AlSi10Mg alloy in different conditions, which were optimized in previous work [6]: (i) T5 (artificial aging (AA) at 160 °C for 4h), (ii) T6B (solubilization (SHT) at 540 °C for 1 h and artificial aging at 160 °C for 4 h), and (iii) T6R (solubilization at 510 °C for 10 min and artificial aging at 160 °C for 6 h). This study highlighted the influence of the morphology, dimension, and distribution of the main microstructural features on the local mechanical behavior of the L-PBF AlSi10Mg alloy in the T5 and T6 conditions. Moreover, these results were correlated with the mechanical behavior of the alloy, particularly the yield strength and the elongation to failure [6].

MATERIAL AND METHODS

AlSi10Mg alloy discs (Fig. 1) (diameter Φ = 46 mm and thickness h = 5 mm) were produced by a SLM500 printing system, using gas atomized powders supplied by Tekna. The discs underwent the heat treatments reported in Table 1 to evaluate the effect of the microstructure on the local mechanical behavior of the material. The process parameters, the chemical-physical features of the powders, and a detailed discussion concerning the choice of the heat treatment parameters are reported in a previous work by the author [6].

The nanoindentation tests were carried out using a Nano-Test Vantage from Micromaterials equipped with a Berkovich indenter (Centerline-to-face angle, α = 65,27°, Young's Module, E_o = 1141 GPa e Poisson coefficient, ν_o = 0.07). A load speed of 1 mN/s, a maximum load of 10 mN, and a holding time of 5 s at the load peak were used. The analysis was carried out using maps with dimensions of 400 x 200 μm to afford the characterization of a large area of material through equidistant indentations at 40 μm. In total, the number of points analyzed in each map was 66.

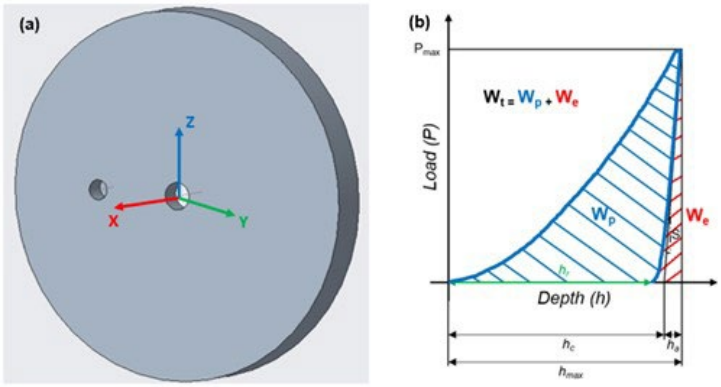

Fig.1 – (a) Representative scheme of the specimens: building axis (z) and plane parallel to the building platform (xy), (b) Load-unload curve for the instrumented indentation technique. / (a) Schema rappresentativo dei provini: asse di costruzione (z) e piano parallelo alla piattaforma di costruzione (xy), (b) Curva di carico-scarico per la tecnica di nanoindentazione strumentata.

Tab.1 – (a) Representative scheme of the specimens: building axis (z) and plane parallel to the building platform (xy), (b) Load-unload curve for the instrumented indentation technique. / (a) Schema rappresentativo dei provini: asse di costruzione (z) e piano parallelo alla piattaforma di costruzione (xy), (b) Curva di carico-scarico per la tecnica di nanoindentazione strumentata.

Condition	T5	T6R	T6B
Heat treatment parameters	Artificial aging (AA) at 160 °C for 4 h, air cooling	Solution (SHT) at 510 °C for 10 min, water quenching at room temperature, Artificial aging (AA) at 160 °C for 6 h, air cooling	Solution (SHT) at 540 °C for 1 h, water quenching at room temperature, Artificial aging (AA) at 160 °C for 4 h, air cooling

Two different parameters were analyzed to correlate microstructure and local mechanical behavior: hardness (H) and elastic recovery parameter (ERP). The first is the ratio between the maximum applied load (P_{max}) and the projected contact area at that load ($A(h_c)$) (Fig. 1.b) [9], which is expressed by eq. 1:

$$H = \frac{P_{max}}{A(h_c)} \quad (1)$$

The elastic recovery parameter (ERP) is a dimensionless index that is indicative of the slope (S) of the unloading curve and consequently related to the ratio between hardness (H) and Young's modulus (E) of the material (Fig. 1.b) [10]:

$$ERP = \frac{h_{max} - h_c}{h_{max}} \quad (2)$$

In eq. 2, h_{max} defines the depth at the maximum load, while hc is the contact depth. The ERP coefficient highlights the elastoplastic behavior of the material: as ERP increases, the elastic work (We) increases, conversely, its decrease in value corresponds to an increase in the plastic work (Wp) [10]. The samples preparation and the data acquisition followed

this procedure: (i) cutting of the samples parallel to the construction axis of the specimens, (ii) embedding of the samples in conductive resin and subsequent metallographic preparation up to polishing with a diamond suspension of 1 μm, according to the ASTM E3 standard, (iii) performing nanoindentation tests, (iv) chemical etching of samples using Weck's reagent (3 g NH_4HF_2, 4 ml HCl, 100 ml H_2O), according to ASTM E407, (v) image acquisition using optical (OM) and field emission gun scanning electron (FEG-SEM) microscopes.

The hardness and ERP data were processed by the Matlab software to create the related maps.

RESULTS

The T5 alloy had no remarkable effects on the microstructure of the AB alloy. Its microstructure is, therefore, characterized by a macrostructure of overlapping MPs (Fig. 2.1) and a substructure of submicrometric cells of supersaturated α-Al surrounded by a eutectic-Si network (Fig. 2.2).

The continuous heating and cooling cycles during L-PBF processing affected the ultrafine cellular structure. In particular, the eutectic-Si network presents different morphologies within the MP structure: (i) quite uniform in the Melt Pool Core (MPC), where the α-Al cells are fine and equiaxial; (ii) larger and more elongated in the areas adjacent to the MPB; (iii) extremely discontinuous in the Heat Affected Zones (HAZ), where it appears fragmented and constituted by small agglomerated Si particles (Fig. 2.3). The hardness and ERP coefficient maps clearly show the effects of the non-uniform microstructure on the mechanical response of the T5 alloy [10]. In particular, it is possible to observe values of H and ERP detected in large HAZ that are approximately 20 ÷ 30% lower than the maximum measured value (H = 1.75 GPa and ERP = 0.062). This confirms the relationship between lower local mechanical properties and a coarser and more inhomogeneous microstructure. In fact, as described by Kim et al. [11], upon loading, dislocations in the Al matrix pile up near the Si-rich interface and lead to the formation of stacking defects resulting in twinning in Si nanoparticles located at the boundaries of Si-rich cells. The morphology and size of the cellular structure influence the hindering mechanism at the eutectic-Si network/α-Al cell interface and consequently the mechanical properties of the alloy. In fact, the lower Si content in the cellular boundaries of the HAZ, resulting from Si decomposing associated with the thermal history of the alloy [12], compared to the fine (MPC) and coarse (MPB) cellular zones (Fig. 2.3), entail less effect in inhibiting dislocation slip. Since dislocations can easily move in the HAZ, hardness decreases while plastic deformation increases. In the tensile test, the plastic deformation is mainly located within the HAZ zones, constrained by the high strength zone (MPC) that prevents the dislocations motion. This leads to a stress-triaxiality condition and the formation and coalescence of micro-voids [6,13,14]. The coalescence of the micro-void and the concentration of the deformation within the HAZ lead to a consequent reduction of ef (Table 2) value and impact toughness of the material [6,15].

The T6R and T6B samples have a completely homogeneous composite-like microstructure consisting of Si particles incorporated into a matrix in the α-Al phase resulting from the SHT phase (Figs. 3.1 and 4.1). However, the different SHT parameters determined variations in the morphology, size, and distribution of the Si particles and, consequently, a different mechanical response, both on the macro-and micro-scale.

In the T6R samples, the homogeneous distribution of the small-sized Si particles and the high cohesion with the α-Al matrix led to the indenter always fully penetrating the α-Al matrix (Figs. 3.4 and 3.5), and therefore the measurements were not affected by scatter. The only off-scale peak values were due to the presence of pores (Figs. 3.2 and 3.3) with a reduction of about 25% in terms of H and ERP.

Conversely, in the T6B samples, the heterogeneous size and distribution of Si particles led to a high difference in both H and ERP values between the particle-free zones (H = 0.8 ÷ 1.0 GPa, ERP = 0.035 ÷ 0.045) (Figs. 4.2, 4.3, and 4.4) and the zones full of large Si particles and/or Si particles clusters in the material (H = 1.4 ÷ 1.7 GPa, ERP = 0.055 ÷ 0.065) (Fig. 4.5). In fact, the measurements on the T6B sample were strongly influenced by the direct interaction of the Berkovich indenter with large Si particles and showed higher hardness and lower ductility in the presence of large Si particles and/or clusters and lower hardness and higher ductility in the Si

particle-free zones. This is in line with the results of the tensile tests (Table 2) and the fracture surface analyses carried out by the author in [6]. The fractographic analyses highlighted that the presence of large Si particles induced a concentration of the plastic flow and the decohesion of the α-Al matrix along their borders as well as the nucleation of large dimples after the Si particle failure due to the local stress field. In the particle-free zones, instead, the presence of homogenous plastic deformation with small dimples was observed [16]. The lower hardness and therefore the tendency to undergo plastic deformation under lower stresses of the particle-free zones could explain the lower YS and ef of the T6B alloy compared to the T6R alloy [17].

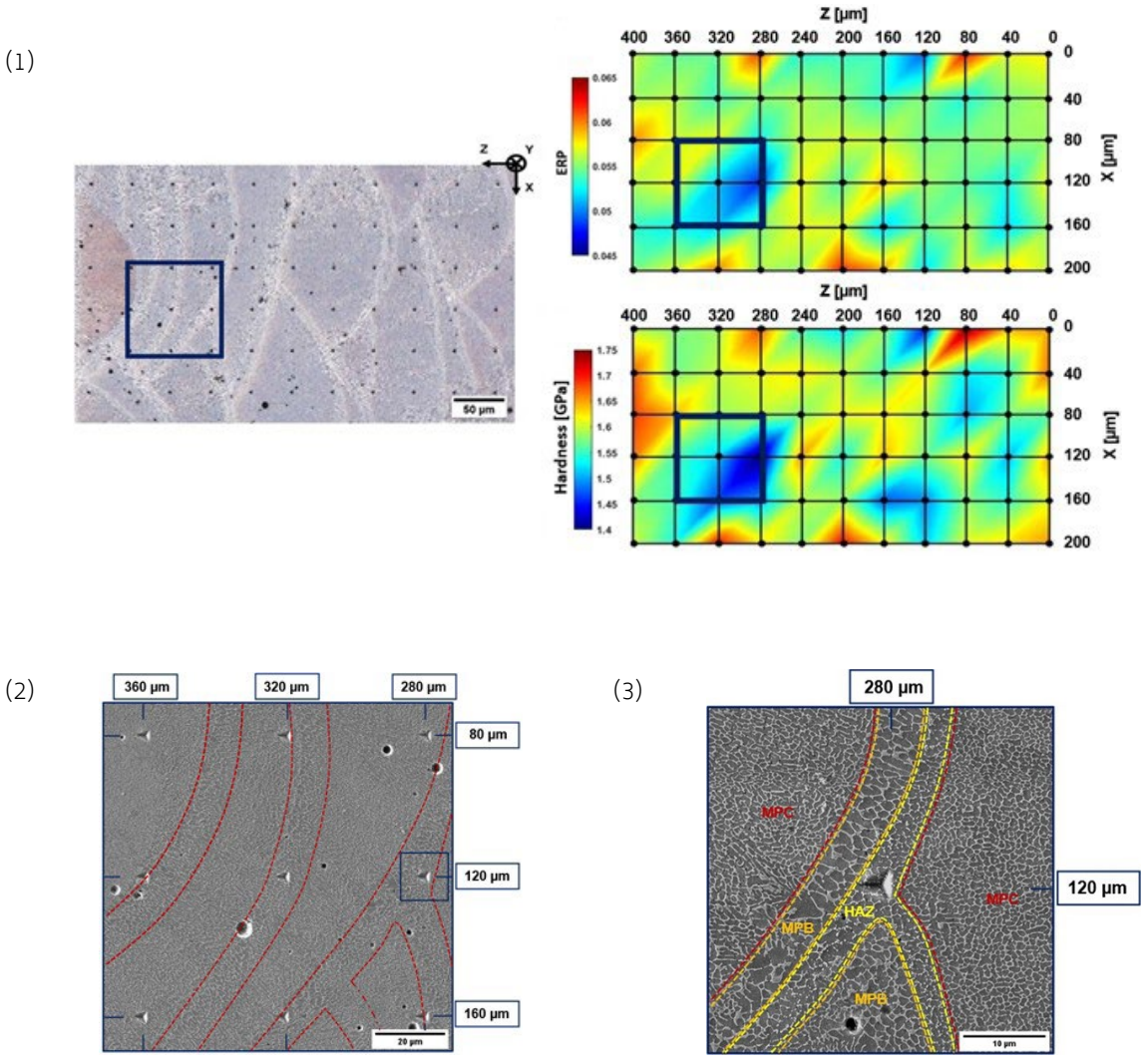

Fig.2 – (1) OM acquisition of the microstructure and nanoindentation matrix for the T5 alloy. The hardness and ERP maps were processed by Matlab software starting from the raw data of the nanoindentation tests; High-magnification microstructures acquired at FEG-SEM: (2) region characterized by a high density of MPB and low hardness and ERP values, (3) HAZ characterized by deep indenter penetration into the Al matrix promoted by the disgregation of the eutectic-Si. / (1) Acquisizione all'OM della microstruttura e della matrice di punti per la lega T5. Le mappe di durezza e ERP sono state elaborate mediante il software Matlab a partire dai dati grezzi della prova di nanoindentazione; Microstrutture ad alto ingrandimento acquisite al FEG-SEM: (2) regione caratterizzata da un'alta densità di MPB e una bassi valori di durezza e coefficiente ERP, (3) HAZ caratterizzata da una profonda penetrazione dell'indentantore nella matrice di Al favorita dalla disgregazione della rete di Si eutettico

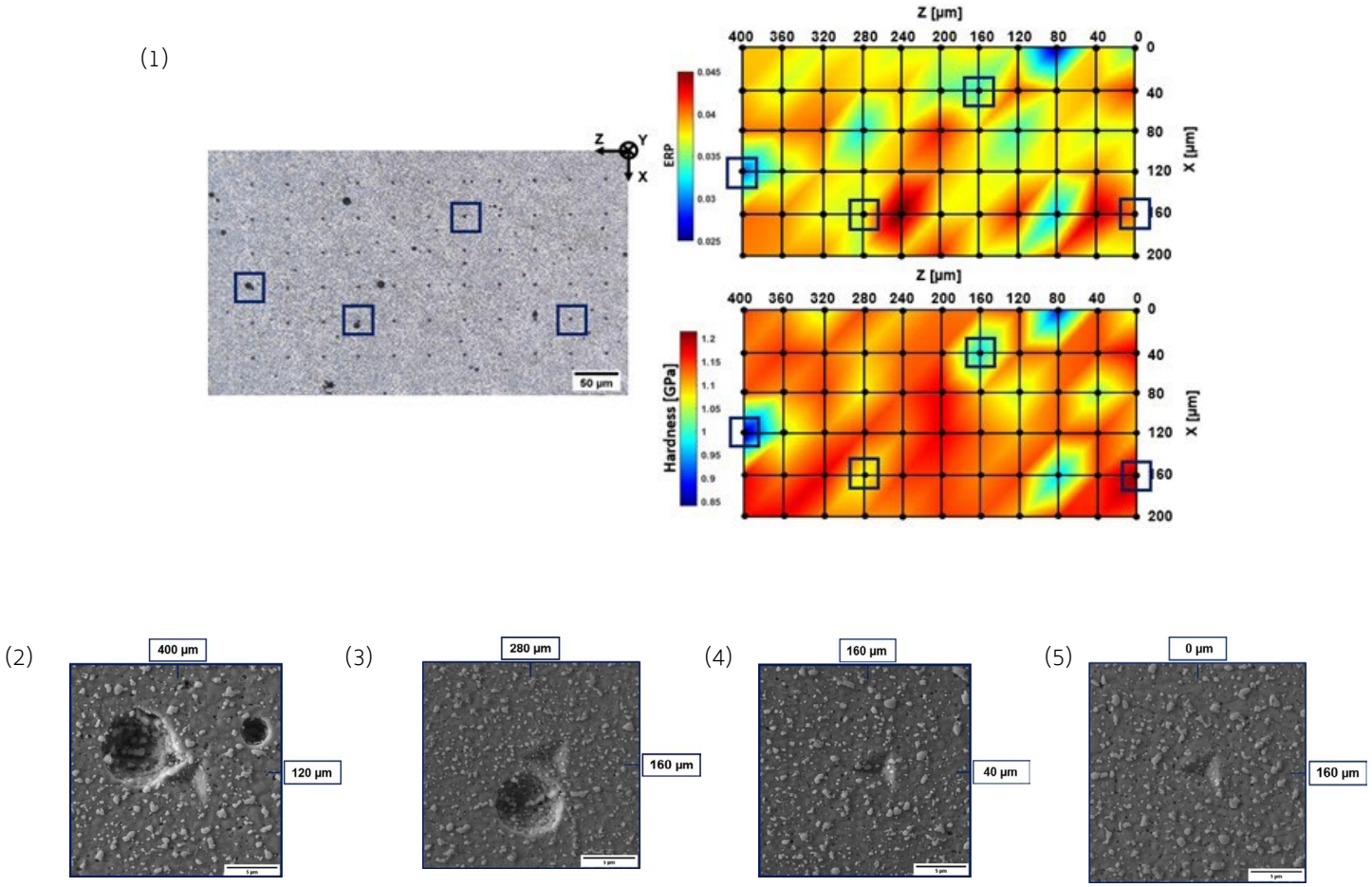

Fig.3 – (1) OM acquisition of the microstructure and nanoindentation matrix for the T6R alloy. The hardness and ERP maps were processed by Matlab software starting from the raw data of the nanoindentation tests; High-magnification microstructures acquired at FEG-SEM: (2) (3) measurements close to porosity and characterized by low hardness and ERP values, (4) (5) areas characterized by a fine dispersion of Si particles and uniform H and ERP values. / – (1) Acquisizione all'OM della microstruttura e della matrice di punti per la lega T6R. Le mappe di durezza e ERP sono state elaborate mediante il software Matlab a partire dai dati grezzi della prova di nanoindentazione; Microstrutture ad alto ingrandimento acquisita al FEG-SEM: (2) (3) rilevazioni in prossimità di porosità e caratterizzate da bassa durezza e basso ERP, (4) (5) aree caratterizzate da una fine dispersione di particelle di Si e da valori di H e ERP uniformi

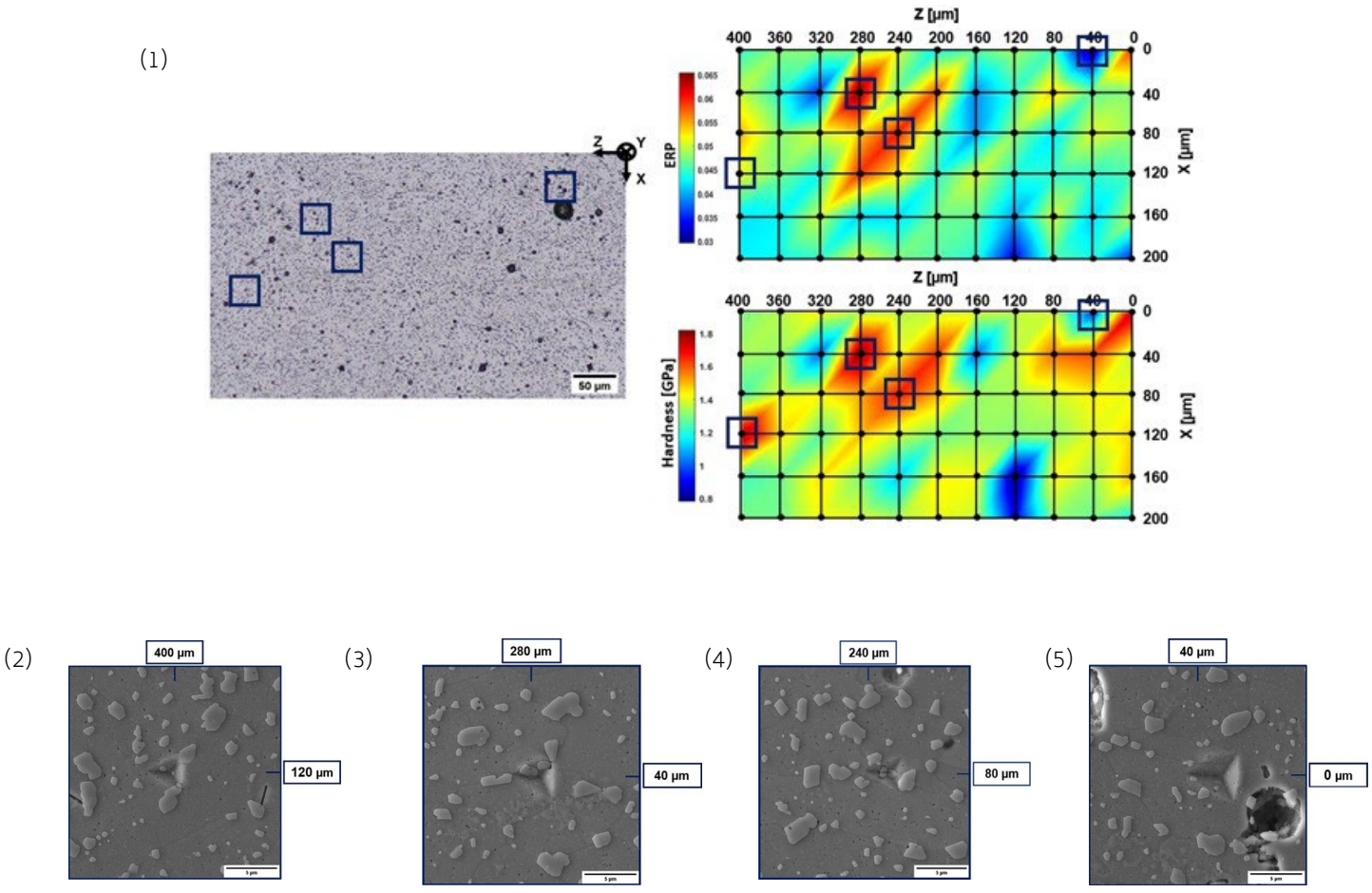

Fig.4 – (1) OM acquisition of the microstructure and nanoindentation matrix for the T6B alloy. The hardness and ERP maps were processed by Matlab software starting from the raw data of the nanoindentation tests; High-magnification microstructures acquired at FEG-SEM: (2) (3) (4) out-of-scale measurements corresponding to areas characterized by clusters of large Si particles, (5) measurement on an area free of large Si particles interacting with the indenter and therefore characterized by low hardness and ERP values / (1) Acquisizione all'OM della microstruttura e della matrice di punti per la lega T6B. Le mappe di durezza e ERP sono state elaborate mediante il software Matlab a partire dai dati grezzi della prova di nanoindentazione; Microstrutture ad alto ingrandimento acquisita al FEG-SEM: (2) (3) (4) rilevazioni fuori scala corrispondenti ad aree caratterizzate da cluster di grandi particelle di Si, (5) rilevazione su di un'area priva di grandi particelle di Si che interagiscono con l'indentatore e caratterizzata da bassi valori di durezza e ERP

Tab.2 - Proprietà meccaniche per le condizioni di trattamento termico analizzate [6] - Mechanical properties for the analyzed heat treatment conditions [6]

	T5	T6R	T6B
YS [MPa]	256 ± 3	251 ± 4	221 ± 6
UTS [MPa]	452 ± 3	319 ± 6	308 ± 7
e_f [%]	4.3 ± 0.6	12.6 ± 0.7	11.8 ± 0.2

CONCLUSIONS

Nanoindentation tests were carried out to evaluate the local mechanical behavior of the L-PBF AlSi10Mg alloy heat-treated in different conditions: T5 (160 °C for 4 h), T6B (540 °C for 1 h + 160 °C for 4 h), and T6R (510 °C for 10 min + 160 °C for 6 h). Based on the obtained results, the following conclusions can be drawn:

- The T5 alloy showed the microstructure characterized by the highest H (1.6 GPa) and ERP (0.055) values. However, a strong local microstructural anisotropy affected the local mechanical behavior of the alloy. The HAZ and the MPB were less effective to inhibit dislocation slip compared to the MPC, thus favoring the plastic deformation in this area and reducing the H and ERP values.
- The T6B and T6R alloys showed lower values of H (1.3 GPa and 1.2 GPa, respectively) and ERP (0.046 and 0.038, respectively), which indicated a softer alloy compared to the T5 alloy. The difference between the two conditions was linked to the size and distribution of the Si particles embedded into the α-Al matrix. While the T6R samples showed a homogeneous mechanical response due to fine dispersion of Si particles, the presence of larger Si particles or clusters in the T6B samples led to a local inhomogeneous mechanical behavior which reflected on the lower YS and ef of the T6B samples compared to T6R ones.

ACKNOWLEDGMENTS AND FUNDING INFORMATION

The present work was supported by the RIMMEL project, CUP B91F18000370009, POR FESR EMILIA ROMAGNA 2014-2020, Asse 1 - Ricerca e Innovazione.

REFERENCES

[1] 1. M. MEHRPOUYA, A. DEHGHANGHADIKOLAEI, B. FOTOVVATI, A. VOSOOGHNIA, S.S. EMAMIAN, A. GISARIO, Applied Sciences, Vol. 9, 3865, (2019).
[2] N. READ, W. WANG, K. ESSA, M.M. ATTALLAH, Materials and Design, Vol. 65, pp. 417-424, (2015).
[3] A. MERTENS, J. DELAHAYE, O. DEDRY, B. VERTRUYEN, J. T. TCHUINDJANG, A. M. HABRAKEN, Procedia Manufacturing, Vol. 47, pp. 1089-1095, (2020).
[4] W. LI, S. LI, J. LIU, A. ZHANG, Y. ZHOU, Q. WEI, C. YAN, Y. SHI, Materials Science and Engineering: A, Vol. 663, pp. 116-125, (2016).
[5] J. FITE, S.E. PRAMEELA, J.A. SLOTWINSKI, T.P. WEIHS, Additive Manufacturing, Vol. 36, 101429, (2020)
[6] G. DI EGIDIO, L. CESCHINI, A. MORRI, C. MARTINI, M. MERLIN, Metallurgical Material Transactions B, Vol. 53, pp. 284–303, (2022).
[7] P.J. MOSES, Q. Liu, J.P. BEST, X. LI, J.J. KRUZIC, U. RAMAMURTY, B. GLUDOVATZ, Acta Materialia, Vol. 211, 116869, (2021).
[8] L. ZHUO, Z. WANG, H. ZHANG, E. YIN, Y. WANG, T. XU, C. LI, Materials Letters, Vol. 234, pp. 196-200, (2019).
[9] J.L. HAY, G.M. Pharr, G.M., ASM Handbook Vol. 8: Mechanical Testing and Evaluation, 10th Edition, ASM International, Materials Park, OH, pp. 232–243, (2000).
[10] M. MUHAMMAD, J.W. PEGUES, N. SHAMSAEI, M, HAGHSHENAS, The International Journal of Advanced Manufacturing Technology, Vol. 103, pp. 4161–4172, (2019).
[11] D.K. KIM, J.H. HWANG, E.Y. KIM, Y.U. HEO, W. WOO, S.H. CHOI, Journal of Alloys and Compounds, Vol. 714, pp. 687–697, (2017).
[12] U. PATAKHAM, A. PALASAY, P. WILA, R. TONGSRI, Materials Science and Engineering: A, Vol. 821, 141602, (2021)
[13] J. DELAHAYE, J. T. TCHUINDJANG, J. LECOMTE-BECKERS, O. RIGO, A. M. HABRAKEN, A. MERTENS, Acta Materialia, Vol. 175, pp. 160-170, (2019).
[14] T.H. Park, M.S. BAEK, H. HYER, Y. SOHN, K.A. LEE, Materials Characterization, Vol. 176, 111113, (2021).
[15] L. LATTANZI, M. MERLIN., A. FORTINI, A. MORRI, G.L. GARAGNANIl, Journal of Materials Engineering and Performance, (2021).
[16] N. TAKATA, M. LIU, H. KODAIRA, A. SUZUKI, M. KOBASHI, Additive Manufacturing, Vol. 33, 101152, (2020)
[17] S. JOSEPH, S. KUMAR, Materials Science & Engineering A, Vol. 588, pp. 111–124, (2013).

Valutazione attraverso nanoindentazione dell'influenza dei trattamenti termici e della conseguente microstruttura indotta sulla risposta meccanica della lega L-PBF AlSi10Mg trattata termicamente

La microstruttura gerarchica della lega AlSi10Mg prodotta tramite tecnologia Laser-based Powder Bed Fusion (L-PBF) determina peculiari caratteristiche microstrutturali e meccaniche. La letteratura scientifica riporta generiche correlazioni fra i principali aspetti microstrutturali e il comportamento meccanico della lega, tralasciando tuttavia l'analisi degli effetti della sub-struttura sul comportamento meccanico locale. Il presente studio ha quindi utilizzato la tecnica della nanoindentazione per determinare l'influenza di differenti condizioni di trattamento termico sulla sub-struttura e sulle proprietà meccaniche della lega L-PBF AlSi10Mg. In particolare, sono stati considerati i seguenti trattamenti termici: T5 (160 °C per 4 h), T6B (540 °C per 1 h + 160 °C per 4 h) e T6R (510 °C per 10 min + 160 °C per 6 h). Lo studio ha evidenziato come piccole variazioni della morfologia o delle dimensioni delle principali caratteristiche microstrutturali abbiano effetto sul comportamento meccanico locale, riflettendosi di conseguenza sul comportamento meccanico complessivo del materiale.

PAROLE CHIAVE: LASER-BASED POWDER BED FUSION (L-PBF), SELECTIVE LASER MELTING (SLM), LEGHE DI AL, ALSI10MG, TRATTAMENTO TERMICO, NANO-INDENTAZIONE, MICROSTRUTTURA, PROPRIETÀ MECCANICHE;